

ANALYSIS OF T₂-D RELAXATION-DIFFUSION NMR MEASUREMENTS FOR PARTIALLY SATURATED MEDIA AT DIFFERENT FIELD STRENGTH

Christoph H. Arns¹, Tariq AlGhamdi¹, Ji-Youn Arns¹,
Lauren Burcaw² and Kathryn E. Washburn³

¹School of Petroleum Engineering, University of New South Wales, Sydney, Australia

²School of Chemical and Physical Sciences, Victoria University of Wellington,
Wellington, New Zealand

³Schlumberger-Doll Research, 1 Hampshire Street, Cambridge, MA 02139

This paper was prepared for presentation at the International Symposium of the Society of Core Analysts held in Halifax, Nova Scotia, Canada, 4-7 October, 2010

ABSTRACT

NMR techniques are usually employed in the petroleum industry to either predict permeability or for fluid typing. Recent advances in NMR measurements saw the development of 2D NMR methods for borehole applications. A particular technique, the transverse relaxation diffusion (T₂-D) NMR correlation measurement, is designed to enhance 1D fluid typing by adding an encoding sequence for the diffusion coefficient of the fluid(s). The fluid type is thus determined by the effective diffusion coefficient; and the environment of the fluid(s) by the diffusion coefficient resolved T₂ relaxation spectrum. In particular, one would expect to be able to determine the wetting fluid, as it would usually respond with a wide range of T₂ relaxation times as compared to the non-wetting fluid, which strongly peaks around the bulk relaxation time.

Uncertainties arise in the interpretation of T₂-D experiments through a) limited signal-to-noise ratio, b) assumptions like weak coupling and surface relaxivity homogeneity in the T₂ domain, c) restricted diffusion and internal gradients mainly in the D domain, and d) assumptions about the separability of the experimental kernel. The inversion of 2D magnetization decays is non-unique and it is desirable to test numerically whether a particular solution is commensurable with the underlying structure if the latter is known.

In this work we consider T₂-D experiments and simulations of those responses on the basis of Xray-CT images of the micro-structure. We carry out T₂-D experiments at different saturations and field strength for fully and partially saturated sandstone and carbonate rock. In the simulations, we track the radius of gyration, internal gradients at Xray-CT resolution, and diffusion averaged internal gradients. We separately account for the different relaxation mechanisms at different field strength. We simulate the NMR T₂-D experiments with a consistent set of material parameters without free parameters across different field strengths and compare to experiment.

INTRODUCTION

NMR T_2 -D correlation experiments are used in the petroleum industry in particular for the purpose of fluid typing. The technique is relatively recent [1,2] and uses the fact that the diffusion coefficient of fluids, e.g. oil and water, are typically quite different to separate the relaxation response of the different fluids using the additional diffusion dimension. This approach essentially enables the application of T_2 relaxation analysis to rocks saturated with more than one fluid while at the same time providing estimates on the fraction and diffusion coefficient of each fluid saturating the pore space.

The T_2 -D experiment consists of two distinct pulse sequences in succession, a diffusion encoding sequence, followed by a Carr-Purcell-Meiboom-Gill (CPMG) sequence used for detection of the signal while also recording the T_2 relaxation decay if a long enough CPMG train is acquired. At high field, usually a pulsed field gradient technique is used for diffusion encoding (stimulated echo). At low field, often a direct echo method is used by combining a short CPMG train with varying time spacing with a T_2 CPMG train with short time spacing [3,4,2]. The short time spacing in the CPMG train recording the T_2 relaxation is chosen to suppress diffusion effects by frequent refocussing of the transverse relaxation. During the diffusion encoding, the application of a strong external gradient, allows us to quickly dephase magnetisation as function of the diffusion coefficient because of the locally varying Larmor frequency, a consequence of the gradient in the magnetic field. However, in rocks, susceptibility differences between rock and fluid components also generate internal magnetic fields [5-9] which contribute to the loss of signal attributed to diffusion. These result in recording an apparent rather than absolute diffusion coefficient spectrum, unless internal gradients are explicitly encoded for [10,11]. If the time spacing during the CPMG T_2 sequence is not short enough, the internal field also influences the T_2 relaxation spectrum resulting in an apparent T_2 relaxation spectrum [20].

An accurate analytic treatment of the T_2 -D NMR response in porous rocks is not easy [9]. To aid quantitative treatment, it is advantageous to model the NMR response numerically. This allows for controlling physical and experimental parameters explicitly, while attempting to match experiment as closely as possible. NMR random walk simulations go as far back as Carr and Purcell in 1954 [12]. Newer treatments include effects of relaxation [13-17], diffusion [18], and internal gradients [19,20] in reservoir rocks. In earlier work, the surface relaxivity typically was treated as a free parameter to match experiments and numerical simulation, leading to much larger surface relaxivity in numerical simulations compared to experiments. Recently, it has been that a consistent set of parameters with a constant surface relaxivity can be used to match experiments and numerical simulations at different field strengths by explicitly modelling the internal magnetic field effect in complex geometries [20]. In this work we extend the approach of [20] for the T_2 relaxation response to T_2 -D responses. We use high-resolution Xray-CT images [16] to define the distribution of the solid and fluid phases of the reservoir rock, and simulate the full experimental pulse sequence, taking into account the static applied field, external gradients, internal gradients as function of the susceptibility of each

component, and surface and bulk relaxation properties of fluids and fluid-fluid and fluid-solid interfaces.

XRAY-CT IMAGE ACQUISITION AND PROCESSING

In this study we consider two benchmark sandstone samples, Bentheimer and Berea sandstone (Figure 1), as well as an oolitic limestone sample, Savonnière limestone (Figure 2). All samples had 5mm diameter and were acquired at about $3\mu\text{m}$ resolution. SEM images were acquired for Savonnière limestone to resolve length scales below Xray-CT resolution. Savonnière limestone contains a significant amount of micro-porosity, some of which is concentrated at rims of ooliths. Macro-pores with very different shapes and a significant amount of heterogeneity are evident. Ooliths which remained intact are unlikely to be saturated by an invading fluid. Partially saturated states are generated by using the maximal sphere transform [21], which is considered to be a reasonable morphological approximation to fluid distributions resulting from spontaneous imbibitions in strongly water-wet porous media [22].

SIMULATION OF NMR RESPONSES

Material properties

We specify a set of material parameters, including the volume susceptibility χ_v of each phase (Table 2), bulk diffusion coefficients D_0 , bulk relaxation times T_{2b} , and hydrogen indices HI of dodecane ($D_{0d}=8\times 10^{-10}\text{m}^2/\text{s}$, $T_{2bd}=1\text{s}$, $\text{HI}_d=1.04$) and saline water ($D_{0w}=2.3\times 10^{-9}\text{m}^2/\text{s}$, $T_{2bw}=1.5\text{s}$, $\text{HI}_w=0.94$), and surface relaxivities ρ between fluids ($\rho_{ow}=\rho_{wo}=0$) and fluids and minerals quartz ($\rho_{wq}=3\mu\text{m}/\text{s}$, $\rho_{dq}=0\mu\text{m}/\text{s}$), calcite ($\rho_{wc}=1\mu\text{m}/\text{s}$, $\rho_{dc}=0\mu\text{m}/\text{s}$), and clay ($\rho_{wk}=10\mu\text{m}/\text{s}$, $\rho_{dk}=0\mu\text{m}/\text{s}$), where q, c, k stands for quartz, calcite, and clay (Figure 3-a). For voxels consisting of one material, the bulk susceptibilities of quartz, calcite, water, or oil are used. For voxels containing a mixture of materials, e.g. in clay regions or for micro-porous voxels, a straight volume-weighted arithmetic average susceptibility is calculated. It is assumed that the clay regions in the sandstones contain 50% clay minerals and 50% water. For clay minerals, we use the bulk susceptibility of Kaolinite. The grey-scale values of the micro-porous voxels in Savonnière limestone were calibrated to porosity in the segmentation process and are considered to be water-saturated, except for fully oil saturated simulations. Their bulk susceptibility is calculated as average of calcite and water fraction for each grey level.

Internal field calculation

The internal magnetic field is calculated in a dipole approximation taking as reference the vacuum. The dipole field \vec{B}_{dip} for $r > a$, a radius of the dipole, is given as

$$\vec{B}_{dip} = \frac{\mu_0}{4\pi} \left[\frac{3(\vec{m}\vec{r})\vec{r} - \vec{m}r^2}{r^5} \right], \quad \vec{m} = \mu_0 \frac{\chi_v}{1 + \chi_v} \vec{B} \approx \mu_0 \chi_v \vec{B}. \quad (1)$$

for a unit volume. Inside the sphere ($r \leq a$) we have

$$\vec{B}_{in} = \frac{2}{3} \mu_0 \vec{m}. \quad (2)$$

The internal magnetic field follows as the convolution of this dipole field with the magnetic susceptibility field. We compare the numerical dipole calculation with the analytical expression in Figure 3-b and show examples of internal field maps of the z-component in Figure 4. It is evident that there is good susceptibility contrast between fluids and solids in the sandstones, except for dodecane-clay region interfaces. The pore size in Berea sandstone is smaller compared to Bentheimer sandstone and internal gradients can be averaged more effectively by diffusion. The susceptibility contrast between dodecane and the matrix for Savonnière limestone is weak.

Micro-porosity modelling

We approximate the sub-resolution response of Savonnière limestone by using the local porosity given by the grey-scale value of the tomographic image after segmentation to define an effective diffusion coefficient proportional to porosity. The hydrogen index of the effective voxels follows directly, and the susceptibility of each voxel is calculated as volume average. It is assumed that local gradients on that scale are effectively averaged.

NMR random walk simulation

The calculations of the NMR responses were carried out on a higher-resolution sub-grid. For each combination of sample, saturation, and Δ, δ times of a DRCOSY sequence [24] three lattice random walks at 2MHz, 12MHz, and 400MHz proton on a 20000^3 lattice (800×25)³ were carried out. We used between 200,000 and 400,000 random walks per simulation, a time step of about 10 μ s, and a total measurement time of 4s (corresponding experimental settings). Simulations were carried out using a grid of 4x4x4 processors.

NMR EXPERIMENTS

High field experiments were carried out on a 400 MHz Bruker MR apparatus using a 15 mm r.f. coil and a Micro 2.5 micro-imaging system. A DRCOSY pulse sequence in the time domain was employed using four different Δ times of 80 ms, 160 ms, 320 ms, and 500 ms, four corresponding δ of 5 ms, 5 ms, 3 ms, and 2 ms respectively, and a 32 gradient step sequence for the first dimension. The second dimension consists of a 1024 echo CPMPG train of ~4s length with an inter-echo spacing of TE=4ms where only even echoes were acquired ($\tau=1$ ms). We measured three rock core samples, Berea sandstone, Savonnière limestone, and Bentheimer sandstone with diameters of 5 mm, 5 mm, and 10 mm respectively. Samples were vacuum saturated with n-dodecane for 1 hour to obtain the oil saturated NMR measurements, and then placed in a 50 kppm NaCl solution for spontaneous imbibition and the NMR measurements were repeated. All experiments were performed at a constant 25°C. These experiments were repeated on a 12 MHz Magritek Halbach MR apparatus using a 25 mm r.f. coil and a quadruple gradient coil. A similar DRCOSY pulse sequence to the 400 MHz sequence was used but had a maximum Δ of 480 ms rather than 500 ms. For the lower field experiments, all δ are kept at 5 ms. The same samples as those in the 400 MHz experiments are used. The same measurements were carried out at low field on a 2Mhz Maran system using sister plugs.

Neglecting cross-terms between internal and external gradients, the T2-D experiment can be characterised by the kernel [3,24]

$$\frac{M(\delta, t)}{M_0} = \sum p(D, T_2) e^{-\gamma^2 D \left\{ \frac{2}{3} \tau^3 g_{\text{int}}^2 + \delta \left(\Delta - \frac{1}{3} \delta \right) g_{\text{ext}}^2 \right\}} e^{-t/T_2} . \quad (3)$$

The 2D inversion of the magnetisation decay for the probability density $p(D, T_2)$ was carried out using a 2D non-negative least square technique with regularisation ignoring the internal gradient contribution to the kernel. Low-field experiments at 2MHz were inverted using the BRD method [1].

RESULTS

We show in Figure 5 simulations for Berea sandstone at low field for three different saturations. The red lines indicate the properties of dodecane used in the simulations, the black horizontal line indicates the diffusion coefficient of water, and the diagonal line indicates hydrocarbons with a spread of diffusion coefficients. The shift and/or splitting of the peak position and the changing weight illustrate the change from low water saturations (Figure 5a) to higher water saturations (Figure 5c) very well. At low water saturations, water as wetting phase is experiencing restricted diffusion, since oil is morphologically assigned to large openings in the pore space. The largest inscribed radius for the wetting phase at $S_w=25\%$ is $\sim 7\mu\text{m}$, which compares with the free diffusion length over a time interval of $\Delta=80\text{ms}$, given as $l_D=(6\Delta D_0)^{1/2}\approx 35\mu\text{m}$. With rising water saturations, the water peak moves to the bulk diffusion coefficient of water. We show in Figure 6 and 7 comparisons between experiments and simulations for oil (Figure 6) and partially saturated samples (Figure 7) at different field strength. At low field a good match with experiment is achieved and a water peak observed (Figure 7). At high field we see higher values for the diffusion coefficients in the simulations, likely caused by an overestimation of internal gradient effects in the simulations: if in Eqn. (3) internal gradients are excluded in the inversion process, D would have to rise (on average) to compensate. It is however unexpected to see the low diffusion coefficients measured in Bentheimer experimentally at high field. Alternative explanations are that cross-terms between internal and external gradients matter e.g. because of local magnetic impurities or that the experimental bandwidth limited the range of diffusion coefficients recorded. In Figure 8, we consider the influence of restricted diffusion on the T₂-D response. For long diffusion times ($\Delta=480\text{ms}$) diffusion coefficients are significantly lower. The same trend can be observed for the numerical results, even though the inversion routine caused pearling in that instance. In Figure 9, we compare measurements of oil saturated Savonnière limestone with preliminary simulations at high field strength. The signal-to-noise ratio of the simulations was not high enough for an inversion to result in sharp spectral features. Increasing Δ results in a slight narrowing of the T₂-D spectrum consistent with diffusion coupling. Here it is important to note that only connected porosity is saturated in the experiments while numerically connectivity at sub-resolution scale was assumed. There is at best a weak peak shift, suggesting that internal gradient effects are negligible for Savonnière limestone.

CONCLUSION

We showed in this work that NMR T_2 -D responses are a sensitive measure of the fluid and susceptibility distribution of reservoir rock. We compared numerical simulations without free parameters to experiments and reproduced main features of the experimental T_2 -D spectra. We made no attempt to match those parameters to experiments. From the numerical results we conclude that further improvements in signal to noise ratio, modelling of experimental limits (e.g. bandwidth), consideration of accurate micro-porosity modelling, fluid distribution, susceptibility heterogeneity, and/or measurement of constituent parameters might be required to exactly match experimental T_2 -D spectra.

ACKNOWLEDGEMENTS

The authors acknowledge the member companies of the ANU/UNSW Digital Core Consortium for their support. We thank Ben Clennell and Joel Sarout for providing the samples for this study. We thank the Australian Partnership for Advanced Computing for generous allocations of computer time. This work is supported by the Australian Research Council through Discovery Grant DP0881112.

REFERENCES

1. Hürlimann, M.D., Venkataramanan, L., and Flaum, C, "The diffusion-spin relaxation time distribution function as an experimental probe to characterize fluid mixtures in porous media", *J. Chem. Phys.*, (2002), **117**, 22, 10223-10232.
2. Hürlimann, M.D., and Venkataramanan, L., "Quantitative measurement of two dimensional distribution functions of diffusion and relaxation in grossly inhomogeneous fields", *J. Magn. Res.*, (2002), **157**, 31-42.
3. Stejskal, E.O., and Tanner, J.E., "Spin diffusion measurements: spin echoes in the presence of a time-dependent field gradient", *J. Chem. Phys.*, (1965), **42**, 288-292.
4. Callaghan, P.T., *Principles of Nuclear Magnetic Resonance Microscopy*, Clarendon Press, Oxford, (1991).
5. Hürlimann, M.D., "Effective Gradients in Porous Media Due to Susceptibility Differences", *Journal of Magnetic Resonance*, (1998), **131**, 232-240.
6. J.L. Shafer, D. Mardon, and J. Gardner, "Diffusion effects on NMR Response of Oil & Water in Rock: Impact of Internal Gradients", (1999), *Society of Core Analysts*, paper SCA-9916.
7. Dunn, K.-J., "Magnetic susceptibility contrast induced field gradients in porous media", *Magnetic Resonance Imaging*, (2001), **19**, 439-442.
8. Dunn, K.-J., Appel, M., Freeman, J.J., Gardner, J.S., Hirasaki, G.J., Shafer, J.L., and Zhang, G., "Interpretation of restricted diffusion and internal field gradients in rock data", (2001), *SPWLA 42nd Annual Logging Symposium*, June 17-20, paper AAA.
9. Wilson, R.C., and Hürlimann, M.D., "Relationship between susceptibility induced field inhomogeneities, restricted diffusion, and relaxation in sedimentary rocks", *J. Magn. Res.*, (2006), **183**, 1-12.

10. Seland, J.G., Washburn, K.E., Anthonsen, H.W., and Krane, J., “Correlations between diffusion, internal magnetic field gradients, and transverse relaxation in porous systems containing oil and water”, *Phys. Rev. E*, (2004), **70**, 51305.
11. Arns, C.H., Washburn, K.E., and Callaghan, P.T., “Multidimensional NMR inverse Laplace spectroscopy in petrophysics”, *Petrophysics*, (2007), **48**, 5, 380-392.
12. Carr, H. Y., and Purcell, E. M., “Effects of diffusion on free precession in nuclear magnetic resonance problems”, *Physical Review*, (1954), **94**, 630-642.
13. Mendelson, K.S., “Percolation model of nuclear magnetic relaxation in porous media”, *Physical Review B*, (1990), **47**, 1081-1083.
14. Wilkinson, D.J., Johnson, D.L., and Schwartz, L.M., “Nuclear magnetic relaxation in porous media: the role of the mean lifetime $\tau(\rho, D)$ ”, *Physical Review B*, (1991), **44**, 4960-4973.
15. Toumelin, E., Torres-Verdin, C., and Chen, S., “Modeling of Multiple Echo-Time NMR Measurements for Complex Pore Geometries and Multiphase Saturations”, *SPE Reservoir Evaluation & Engineering*, (2003), **8**, 234-243.
16. Arns, C.H., Sheppard, A.P., Sok, R.M., and Knackstedt, M.A., “NMR petrophysical predictions on digitized core images”, *Petrophysics*, (2007), **48**, 3, 202-221.
17. Talabi, O., Alsayari, S., Fernø, M.A., Riskedal, H., Graue, A., Blunt, M.J., “Pore-scale simulation of NMR response in carbonates”, (2008), *Society of Core Analysts*, Abu Dhabi, UAE.M.D, paper SCA2008-30.
18. Zhang, G.Q., and Hirasaki, G.J., “CPMG relaxation by diffusion with constant magnetic field gradient in a restricted geometry: numerical simulation and application”, *J. Magn. Res.*, (2003), **163**, 81-91.
19. Zhang, G.Q., Hirasaki, G.J., and House, W.V., “Internal field gradients in porous media”, *Petrophysics*, (2003), **44**, 6, 422-434.
20. Arns, C.H., Melean, Y., Burcaw, L., Callaghan, P.T., and Washburn, K.E., “Comparison of experimental NMR measurements with simulated responses on digitized images of mono-mineralic rocks using Xray-CT”, (2009), *Society of Core Analysts*, paper SCA2009-44.
21. Thovert, J.-F., Yousefin, F., Spanne, P., Jacquin, C.G., and Adler, P.M., “Grain reconstruction of porous media: Application to a low-porosity Fontainebleau sandstone”, *Phys. Rev. E.*, **63**, no. 061307, 17 pages.
22. Munish, M., Senden, T.J., Sheppard, A.P., Middleton, J.P., and Knackstedt, M.A., “Visualizing and quantifying the residual phase distribution in core material”, (2009), *Society of Core Analysts*, paper SCA2009-16.
23. Potter, D.K., AlGhamdi, T.M., and Ivakhnenko, O.P., “Sensitive carbonate reservoir rock characterization from magnetic susceptibility: mineral quantification, correlation with petrophysical properties, and anisotropy”, (2008) *Society of Core Analysts*, paper SCA2008-10.
24. Galvosas, P., Qiao, Y., Schönhoff, M, and Callaghan, P.T., “On the use of 2D correlation and exchange NMR spectroscopy in organic porous materials”, *Magnetic Resonance Imaging*, (2007), **25**, 497-500.

Table 1: Symbols and abbreviations. Subscripts to symbols used in the text are w (water), d (dodecane), q (quartz), k (clay), c (calcite).

Symbol	Meaning	Symbol	Meaning
a	Length unit	M_0	Initial magnetisation
B_{dip}	Magnetic dipole field	μ_0	Magnetic permeability
Δ	Diffusion interval in PGSE	r	Sphere radius
δ	Gradient time in PGSE	ρ	Surface relaxivity
D_0	Bulk diffusion coefficient	S_w	Water saturation
γ	Gyromagnetic ratio	t	Time
g_{int}	Internal magnetic field gradient	τ	Time between 90° and 180° pulse in CPMG echo train
g_{ext}	External magnetic field gradient		
HI	Hydrogen index	T_{2b}	Fluid bulk relaxivity
l_D	Diffusion length	TE	CPMG inter-echo time spacing
m	Magnetic moment	χ_v	Volume magnetic susceptibility (SI)
M	Magnetisation decay		

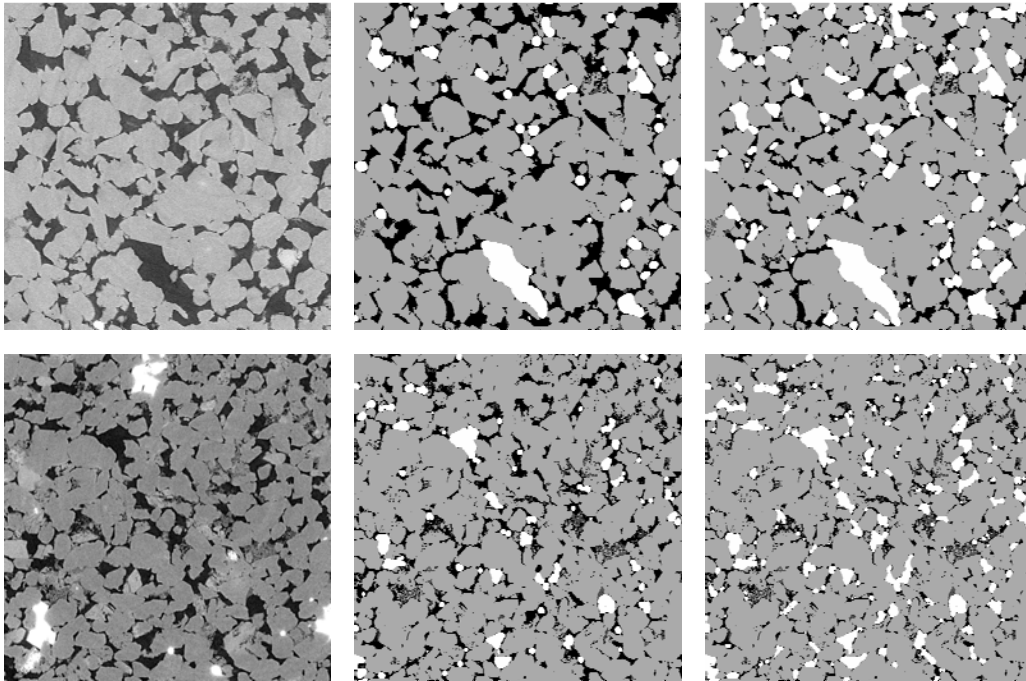


Figure 1: Slices through tomograms and derived phase distributions of the sandstone samples used in this study. Top: Bentheimer sandstone (FOV: 800^2 voxel, resolution: $2.89 \mu\text{m}$, total porosity 0.239, resolved porosity 0.232). Bottom: Berea sandstone (FOV: 800^2 voxel, resolution: $2.84 \mu\text{m}$, total porosity 0.18, resolved porosity 0.179). Left: grey-scale tomograms. Middle and right: tomograms segmented into quartz (grey), clay region (dark grey), and pore space (black and white). The pore space is partitioned into two fluids using a morphological approximation to fluid distributions, white being the non-wetting fluid. Wetting fluid saturations are 75% (middle) and 50% (right).

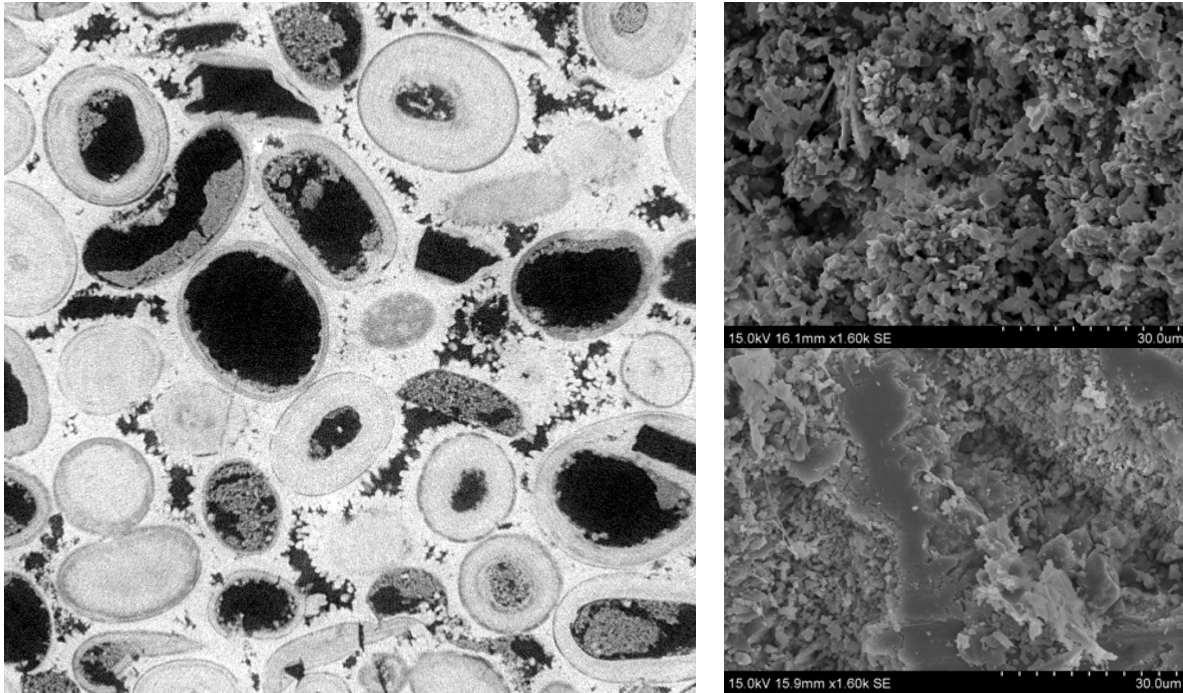


Figure 2: Top: Slices through the 3D simulation domain of Savonnière limestone (FOV: 800^2 voxel, resolution: $2.81 \mu\text{m}$). Left: X-ray-density map. Right: A close-up of the centre of an oolith (top) and a contact between ooliths (bottom) using a Hitachi S3400 SEM fitted with secondary and backscatter electron detectors that allow for topographic and compositional (atomic number contrast) surface imaging of samples. The individual ooliths are stronger and tend to remain in their little sparry cups at the cut surface. It is likely that some oolith centers therefore will not be in communication with an invading fluid. Total imaged porosity (including grey-scale micro-porosity): 0.258, image resolved “macro” porosity 0.186.

Table 2: Mineral and fluid susceptibilities used to calculate effective susceptibilities [25].

Material	Mass Magnetic Susceptibility ($10^{-8} \text{ m}^3 \text{ kg}^{-1}$)	Volume Magnetic Susceptibility (10^{-5})
Quartz, SiO_2	-0.6191	-1.641
Calcite, CaCO_3	-0.4839	-1.311
Kaolinite, $\text{Al}_2[\text{Si}_2\text{O}_5](\text{OH})_4$	-0.6474	-1.68
Water, H_2O	-0.9051	-0.9035
Dodecane, $\text{C}_{12}\text{H}_{26}$	-1.68	-1.26
50kppm NaCl brine		-0.935
Clay region, 50% brine		-1.31

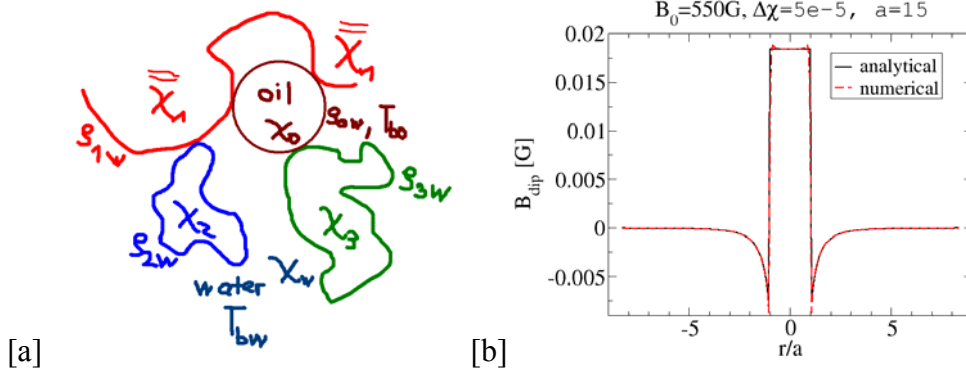


Figure 3: Illustration of the use of material properties in the numerical calculations of the NMR response for three solid phases (numbered) and two fluid phases (water and oil). [a] Sketch of the material property distributions for a multi-mineral multi-fluid phase distribution. [b] Dipole profile calculated numerically versus the analytical formula on a regular grid for a given susceptibility contrast.

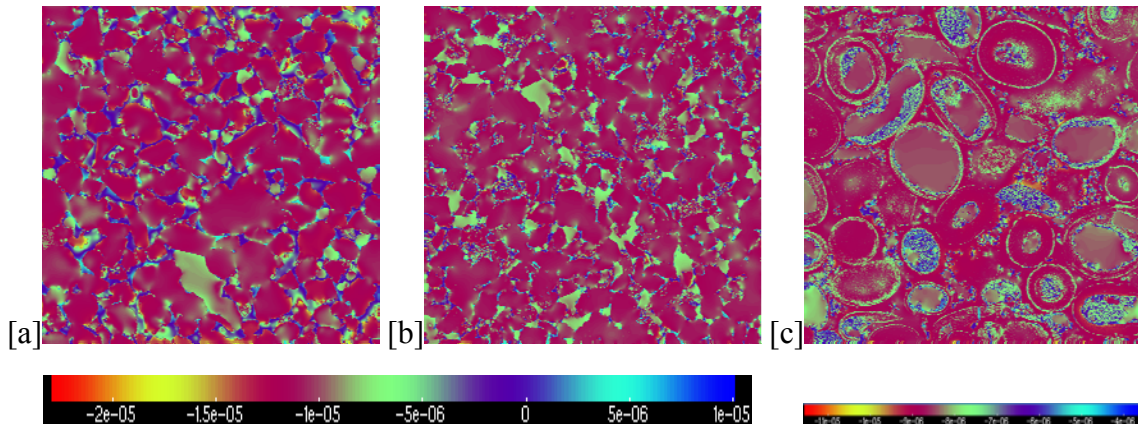


Figure 4: Slices through the coarse scale ($\sim 3 \mu\text{m}$ resolution) internal magnetic fields of the 800^3 simulation domain in units of B_0 perpendicular to $B_0 = (0,0,B_0)$ for [a] Bentheimer sandstone, [b] Berea sandstone, and [c] Savonnière limestone.

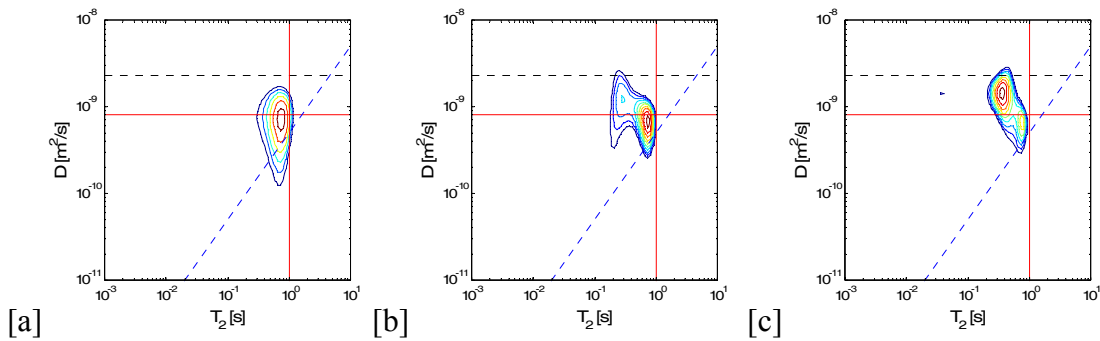


Figure 5: T_2 - D simulations for Berea sandstone at low field (2MHz) and diffusion interval $\Delta=80\text{ms}$. [a] $S_w=25\%$, [b] $S_w=50\%$, [c] $S_w=75\%$.

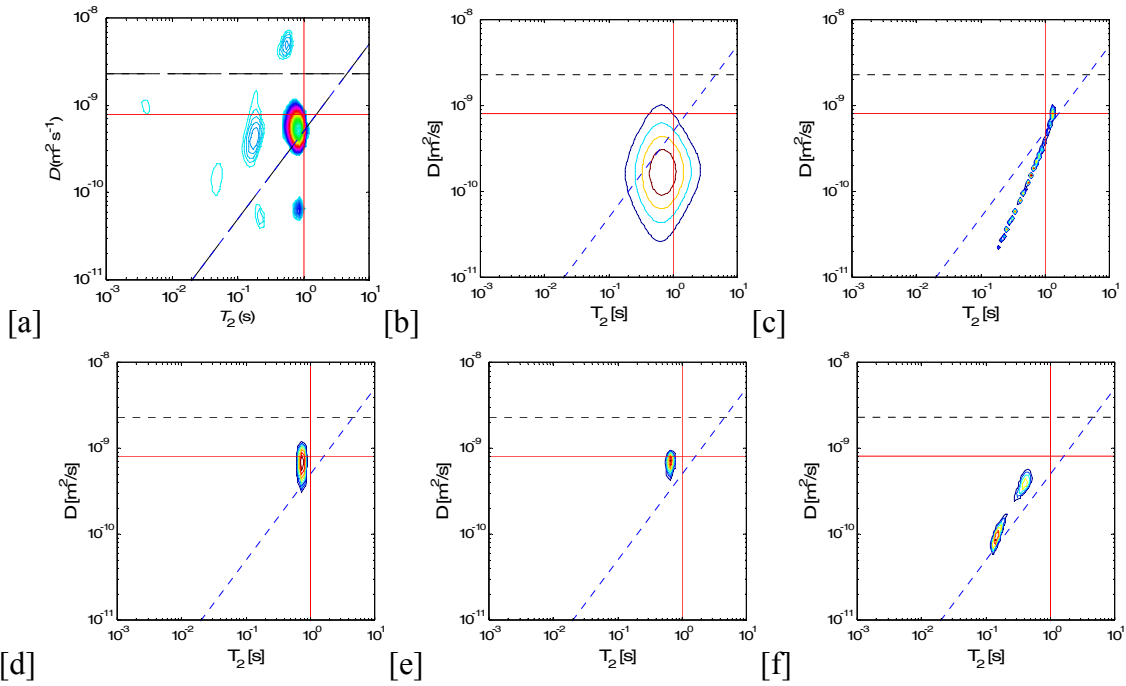


Figure 6: T_2 - D plots for oil-saturated Bentheimer sandstone. [a,d] 2MHz, $\Delta = 40$ ms, [b,e] 12MHz, $\Delta = 80$ ms, [c,f] 400MHz, $\Delta = 80$ ms. Top: experiment. Bottom: Simulation.

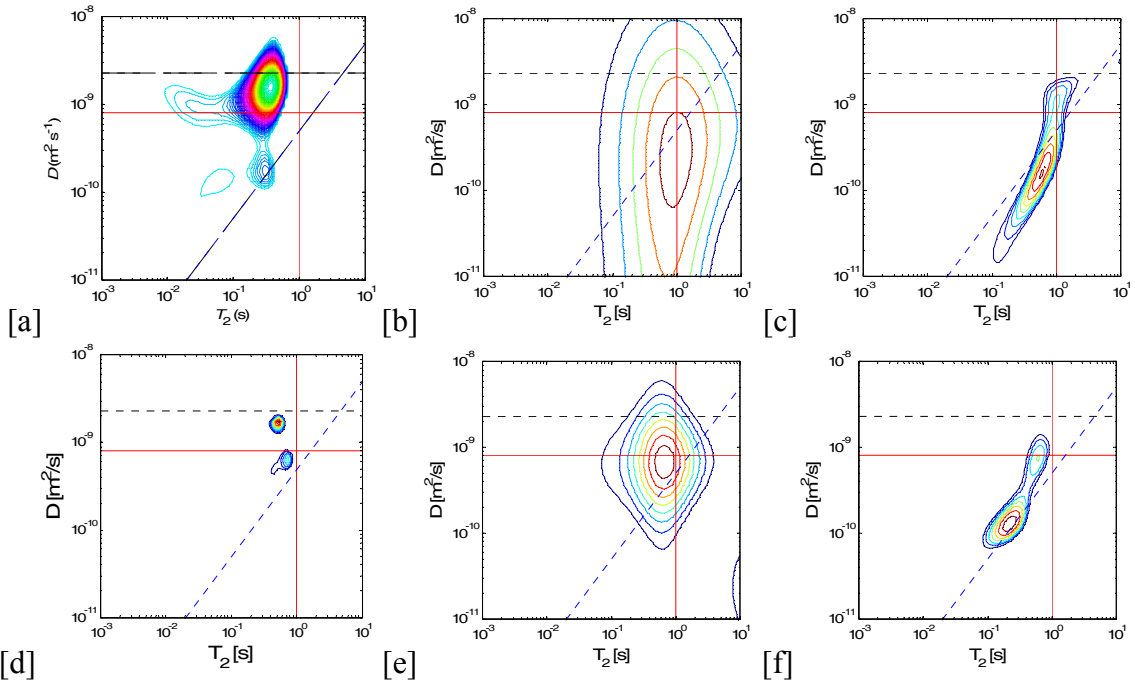


Figure 7: Bentheimer sandstone, partially saturated. [a] 2MHz, $\Delta = 40$ ms, [d] 2MHz, $\Delta = 160$ ms, $S_w=75\%$, [b,e] 12MHz, $\Delta = 80$ ms, [c,f] 400MHz, $\Delta = 80$ ms. Top: experiment. Bottom: Simulation ($S_w=25\%$).

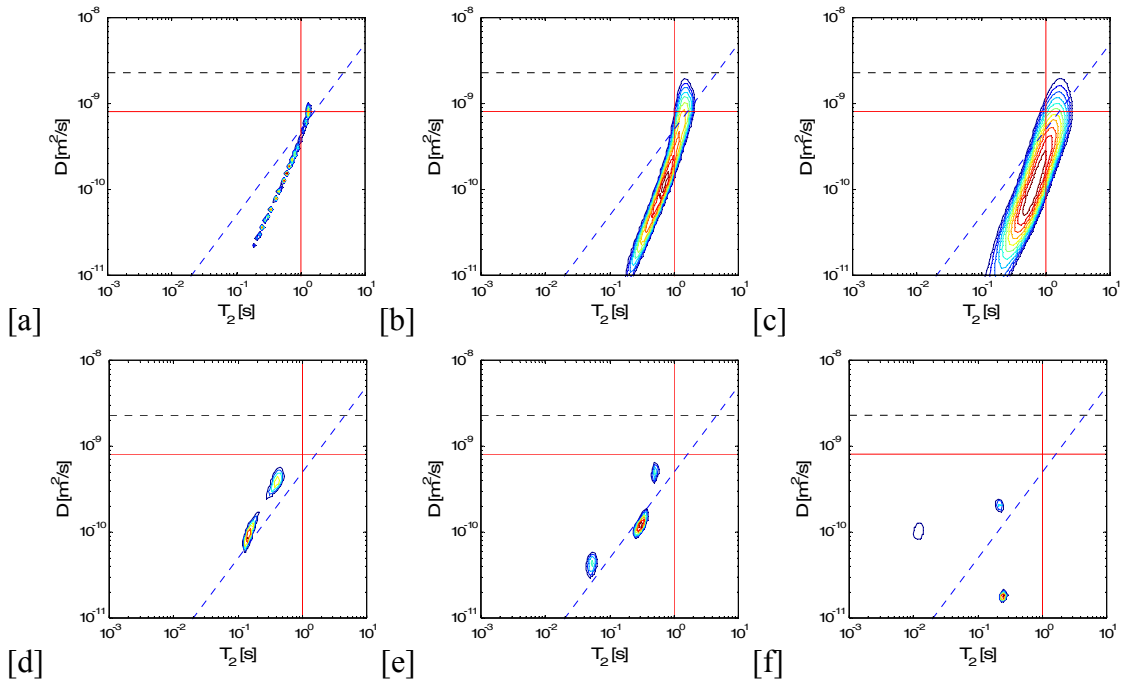


Figure 8: High-field (400MHz) T_2 -D plots for oil-saturated Bentheimer sandstone and three diffusion intervals $\Delta = 80\text{ms}, 160\text{ms}, 500\text{ms}$. Top: experiment. Bottom: simulation.

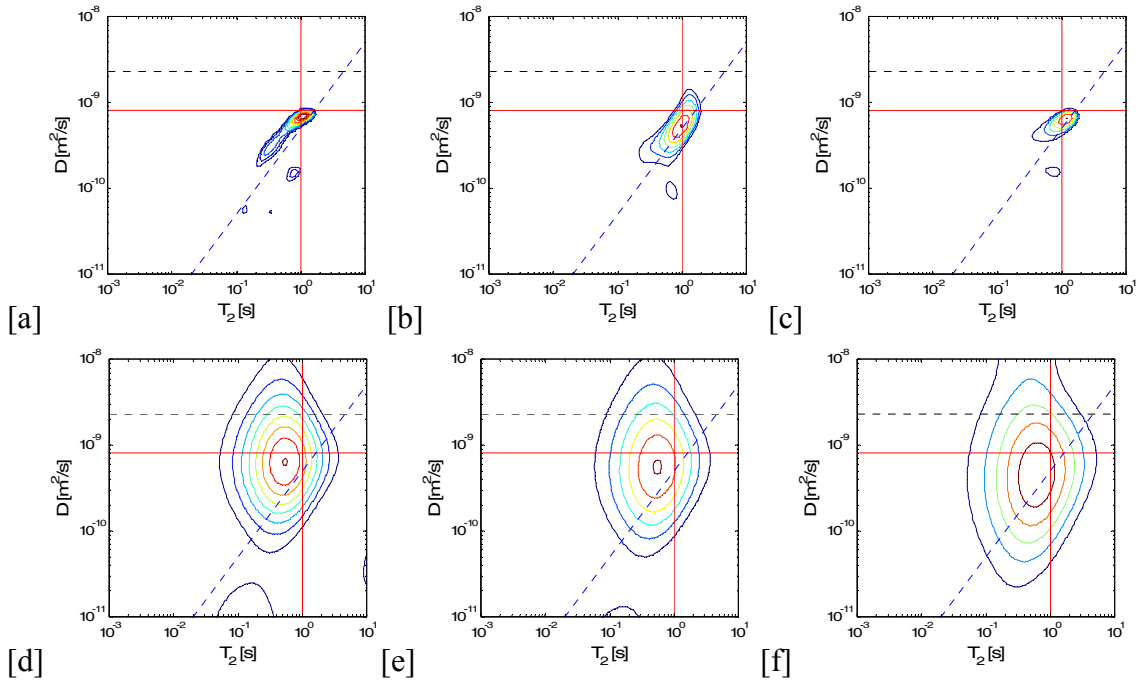


Figure 9: High-field (400MHz) T_2 -D plots for oil-saturated Savonnière limestone and three diffusion intervals $\Delta = 80\text{ms}, 160\text{ms}, 500\text{ms}$. Top: experiment. Bottom: simulation.